Article ID: 1006-8775(2019) 02-0201-10

SENSITIVITY OF THE WEATHER RESEARCH AND FORECASTING MODEL TO RADIATION SCHEMES IN CHINA

WANG Yong-li (王永立)[1, 2], FENG Jin-ming (冯锦明)[1], ZHENG Zi-yan (郑子彦)[1], JIN Shao-fei (靳少非)[3]
(1. CAS Key Laboratory of Regional Climate-Environment for Temperate East Asia, Institute of Atmospheric Physics, Chinese Academy of Sciences, Beijing 100029 China; 2. Institute of Environment, Energy and Sustainability, The Chinese University of Hong Kong, Hong Kong, China; 3. Department of Geography, Ocean College, Minjiang University, Fuzhou 350108 China)

Abstract: Results of one-year simulations using the Weather Research and Forecasting (WRF) model, with the use of different radiation schemes (RRTM, RRTMG, CAM, New Goddard and Goddard), are evaluated for China. The observations used in the model assessment include station data from the China Meteorological Administration, 14 flux field sites arranged in a coordinated observation network, and Global Land Data Assimilation System (GLDAS) data. Specifically, based on a Taylor diagram, the temperature differences between the radiation schemes are small, and the best annual mean spatial pattern and average value for China as a whole is produced by RRTMG. For the rainfall and net radiation annual mean simulation, the New Goddard and CAM schemes present better results than the RRTMG scheme. With respect to low cloud cover, all the schemes have similar reproduction without high cover on east of Tibet Plateau. Overall, the New Goddard and CAM schemes are suitable for longtime simulation without nesting and nudging options.

Key words: radiation schemes; WRF; regional climate
CLC number: P435 **Document code:** A
doi: 10.16555/j.1006-8775.2019.02.007

1 INTRODUCTION

Numerical models, including both global climate models and regional climate models, consist of various physical parameterizations and land surface schemes. They incorporate numerous options for physical parameterizations of convection, radiation, cloud microphysics and other processes. Of the abovementioned parameterizations, critical consideration should be given to the radiation processes for the simulation on sub-seasonal to annual timescales; at these timescales, the radiative heating rate may be significant, compared to the advection and convection (Giorgi and Mearns [1]). Longwave and shortwave radiation are fundamental driving forces on seasonal or longer timescales for numerical simulation (Kim et al.[2]).

The Weather Research and Forecasting (WRF) model offers multiple physics options (planetary boundary layer (PBL), land surface model (LSM), microphysics (MP), cumulus schemes (CU), radiation schemes, etc.) that can be combined in any way. The abovementioned parameterizations in WRF range from simple to more sophisticated options. Depending on the model domain, spatial resolution, location, and intended application, researchers have reported different simulation performances using different combinations of physical schemes to simulate atmospheric processes(Feng et al.[3, 4]; Heath and Fuelberg[5]).

The WRF surface layer is the first vertical layer for which friction velocities and exchange coefficients are calculated. Then the results are used by land-surface models to evaluate surface heat and moisture fluxes, which are also employed in planetary boundary layer to calculate surface stress. The surface fluxes and surface diagnostic fields are assessed in the surface layer over the water bodies. The LSM, which gets atmospheric information from other schemes, provides the land-surface fluxes of heat and moisture to the PBL. The PBL schemes are used to parameterize the unresolved turbulent vertical fluxes of heat, momentum in vertical (Hu et al. [6]). Different PBL schemes adopt different assumptions regarding the transport of mass, moisture, and energy, which may lead to differences in the boundary layer and subsequently the whole model domain (Bank et al. [7]; Cohen et al. [8]; Huang et al. [9]; Wang et al. [10]; Zhang et al. [11]). The surface convective rainfall is derived from the cumulus parameterization (CP) which is responsible for estimating the rate of sub-grid-scale convective precipitation, the release of latent heat, and the redistribution of heat, moisture, and

Received 2017-12-20; **Revised** 2019-01-03; **Accepted** 2019-05-15
Foundation item: National Key Research and Development Program of China (2016YFA0600403)
Biography: WANG Yong-Li, Ph. D., Associate Researcher, primarily undertaking research on numerical simulation.
Corresponding author: FENG Jin-ming, e-mail: fengjm@tea.ac.cn

momentum in the vertical direction (Arakawa[12]; Kain and Fritsch[13]). Cumulus convection is intended to represent the large-scale temperature and moisture fields through unresolved updrafts and downdrafts (Arakawa and Schubert[14]; Zhang et al.[15]). The microphysical scheme includes explicitly resolved water vapor, cloud and rainfall processes which provide non-convective rain to the LSM and interact with radiation schemes by cloud effects.

A simulation of particular process should be focused on the depiction of tropospheric surface exchanges of heat, moisture, and momentum (PBL, LSM, CU, MP) which usually occur on the hourly or daily time scales. Besides, it is more convincing to use suitable radiation physical considerations in regional climate models (RCMs) when simulating climate change, because the radiation heating rate could take effect on month-to-year time scales[1].

The outline of the paper and the main results are organized as follows. Following the introduction, section 2 highlights the characteristics of the different radiation schemes. A description of the model and the design of the sensitivity experiments are presented in section 3. The sensitivity results to different radiation schemes are illustrated and discussed in section 4. The last section provides general conclusions and suggestions for further analyses.

2 DESCRIPTION OF THE RADIATION SCHEMES

The radiation schemes in WRF are tailored to evaluate the atmospheric heating rate due to radiative flux divergence and downward shortwave and longwave radiative flux for the ground heat budget. The radiation considered includes wavelengths from the ultraviolet to the infrared through the visible solar spectrum, as well as the absorption, reflection, and scattering processes that take place in the atmosphere and at the surface. The radiation process responds to the specified carbon dioxide, ozone and (optionally) trace gas concentrations, as well as model-predicted cloud and water vapor distributions. Many radiation schemes contain longwave schemes and also include shortwave schemes. There are two separate shortwave schemes (Dudhia, Goddard), a single longwave scheme (RRTM) and three schemes that combine short- and long-wave schemes (New Goddard, CAM, RRTMG).

The Dudhia shortwave scheme is a simple downward integration that allows efficient assessment of clouds and clear-sky absorption and scattering, which is directly taken from the Fifth-Generation NCAR/Penn State Meso-scale Model (MM5) (Dudhia[16]). This scheme uses look-up tables for cloud albedo and absorption (Stephens[17]). It is a simple broadband model, and is limited in scope to the evaluation of global horizontal irradiance at various vertical levels.

The Goddard shortwave scheme is a two-stream multi-band scheme that includes 11 spectral bands, ozone is considered from climatological profiles and cloud effects (Chou et al.[18]) and that employs a modified delta-Eddington approximation. The maximum-random assumption is applied for treating overlapping clouds. Clouds are grouped into high, middle, and low clouds, which are separated by the level indices.

RRTM is the abbreviation of Rapid Radiative Transfer Model longwave scheme, which is a rapid and accurate correlated-k radiative transfer model. The primary objective of RRTM is to obtain accuracy in the calculation of fluxes and cooling rates (Iacono et al.[19]). For a given atmosphere, this scheme calculates the indices and fractions related to the pressure and temperature interpolations.

The New Goddard short- and long-wave scheme contain a strict threshold of cloud optical depth (=0.0001) for cloud flags in order to account for thin-cloud radiative effects. Beyond that, the New Goddard scheme has a correct two-stream adding approximation in diffuse transmissivity (http://www.mmm.ucar.edu/wrf/users/workshops/WS2007/presentation/5-1_Shi.pdf).

The RRTMG short- and long-wave scheme, which is developed at Atmospheric and Environmental Research (AER), is initially implemented as a WRF radiation option in 2009. RRTMG utilizes the McICA (Monte-Carlo Independent Column Approximation) (Raisanen et al.[20]), which is an efficient statistical method for representing sub-grid scale cloud variability, including cloud overlap. RRTMG also employs the correlated k-distribution radiative transfer technique and a two-stream method accounting for the multiple scattering, and it is an accelerated and advanced version of RRTM (Iacono et al.[21]).

The CAM shortwave and longwave scheme in WRF are from the Community Atmosphere Model (CAM3) climate model, which is used in the Community Climate System Model (CCSM). The CAM short- and long-wave scheme uses yearly CO_2 concentration and includes a mechanism for treating the slow variations in the solar constant over the 11-year cycle for longer secular trends. An updated parameterization of near-infrared absorption by water vapor and the inclusion of prescribed aerosol data sets for computing shortwave aerosol radiative forcing are the other important characteristics of CAM (Neale et al.[22]). The delta-Eddington approximation is also employed for solar radiative transfer and is coupled with an absorptivity-emissivity formulation for IR (infrared radiation) radiation transfer.

The longwave radiation schemes utilized in the present WRF model either use preset tables to represent longwave processes due to water vapor, ozone, carbon dioxide, and trace gases (if present), as well as accounting for cloud optical depth (in the RRTM scheme), or follow the simplified exchange method, which performs calculations over the spectral bands associated with carbon dioxide, water vapor, and ozone (ETA GFDL

longwave scheme) (Gu et al.[23]).

3 WRF MODEL SIMULATIONS USING DIFFERENT RADIATION SCHEMES

3.1 *Model configuration and experimental design*

In this paper, the advanced research version of WRF (version 3.3) is used to simulate the regional impacts of different radiation schemes on climate change. In terms of physical options, we use the WRF Single-Moment 3-class scheme (WSM3) microphysical parameterization(Hong et al[24]); the new Kain-Fritsch convective parameterization (Kain[25]); the Yonsei University(YSU)planetary boundary layer (PBL) scheme (Hong et al.[26]); and the Noah land surface model(Chen and Dudhia[27]). The different shortwave and longwave radiation schemes are listed in Table 1. Except for the different design described in detail in section 2, the RRTMG and CAM radiation schemes are selected because these two schemes usually are used in regional simulation (Saide et al. [28]; Yang et al. [29]; Yu et al.[30]), the New Goddard scheme is the update scheme of Goddard (Montornes et al.[31]), and the default radiation option in WRF model is Dudhia and RRTM scheme.

Table 1. Experimental design.

Case	CO_2 (ppmv)	Longwave Radiation	Shortwave Radiation
Exp1	330	RRTM	DUDHIA
Exp2	330	RRTM	GODDARD
Exp3	337	New GODDARD	New
Exp4	330	CAM	CAM
Exp5	285	RRTMG	RRTMG
Exp6	330	RRTMG	RRTMG
Exp7	379	RRTMG	RRTMG

The initial conditions and boundary conditions (ICBCs) for the large-scale atmospheric fields (i.e., temperature), sea surface temperature (SST), and initial soil parameters (i.e., soil water and soil moisture) are obtained from the National Centers for Environmental Prediction (NCEP) global forecast system (GFS) final (FNL) operational global analysis data, which are available on a 1°×1° global grid starting in 1999 at a temporal frequency of 6 hours. The Lambert conformal conic projection is used as the model horizontal coordinates, with the standard parallel at 105°E. In terms of the vertical coordinates, 28 terrain-following eta levels that extend from the surface to 50 hPa are used. The model simulations, which have a time step of 180 seconds, extend from December 2007 to December 2008, and the boundary data are updated every 6 hours. The model outputs results are updated every 6 hours, and these results are used for model evaluation.

3.2 *Evaluation data*

The data for model validation includes China Meteorological Administration 2-m temperature and rainfall (Xie et al. [32]; Xu et al.[33]), as well as land surface products simulated by four land surface models (Noah) from the Global Land Data Assimilation System (GLDAS) (https://disc.sci.gsfc.nasa.gov/datasets/GLDAS_NOAH025_M_V2.1/summary?keywords=GLDAS).The ERA-Interim cloud data is the latest global atmospheric reanalysis produced by the European Center for Medium-Range Weather Forecasts (ECMWF). The ERA-Interim project is conducted in part to prepare for a new atmospheric reanalysis to replace ERA-40, which will extend back to the early part of the twentieth century (Dee et al.[34]).

Latent heat flux and sensible heat flux data are collected from the 14 field eddy covariance (EC) flux sites, which are part of a coordinated enhanced observation project that includes arid and semi-arid regions in northern China (Table 2). These 14 flux sites represent the dominant vegetation/land cover types in the region: temperate grassland, cropland, deciduous broadleaf forests, and evergreen needleleaf forests (Wang et al. [35]). Intensive calibration and maintenance are carried out weeks before the coordinated enhanced observation period (July to September) to ensure instrument performance and data quality. Quality and error checking procedures are performed regularly to maintain continuous, high-quality measurements. The data over these three months are used to study the heat flux component from the different radiation simulation results (Hou et al.[36]). The simulation areas and the EC flux sites are shown in Fig. 1.

4 RESULTS

4.1 *Validation by circulation pattern*

Land surface processes are mainly driven by precipitation and solar radiation, which also exert information back to the atmosphere through surface energy, water vapor and momentum fluxes(Zeng et al.[37]). The circulation pattern change would lead to the change in transportation of energy and moisture. Based on the spatial distribution of relative humidity and wind on 850 hPa between ERA-Interim and different radiation schemes (Figure not shown), it is found that the largest seasonal difference occurs in the summer time, while the smallest one in the winter time. Among the different radiation schemes, on either the annual mean or seasonal

Table 2. Main characteristics of the 14 flux sites within the study region.

Site	Vegetation Type	Location	Elevation (m)
JZ	Cropland (maize)	41°09 N, 121°12 E	17
YK	Cropland (maize)	38°51 N, 100°15 E	2859
LZ	Cropland (maize)	39°20 N, 100°25 E	1382
TYC	Cropland (sunflower)	44°35 N, 122°52 E	151
DX	Cropland (wheat)	35°33 N, 104°36 E	1912
ZY	Steppe desert	39°05 N, 100°16 E	1483
DS	Desert steppe	44°05 N, 113°34 E	990
TYG	Degraded meadow steppe	44°34 N, 122°55 E	151
AR	Sub-alpine meadow steppe	38°03 N, 100°28 E	3033
YZ	Typical steppe	35°57 N, 104°08 E	1968
NM	Desert steppe	42°56 N, 120°42 E	371
DYK	Evergreen needleleaf forest	38°32 N, 100°15 E	2823
CW	Deciduous broadleaf forest	35°15 N, 107°41 E	1220
MY	Deciduous broadleaf forest	40°38 N, 117°19 E	350

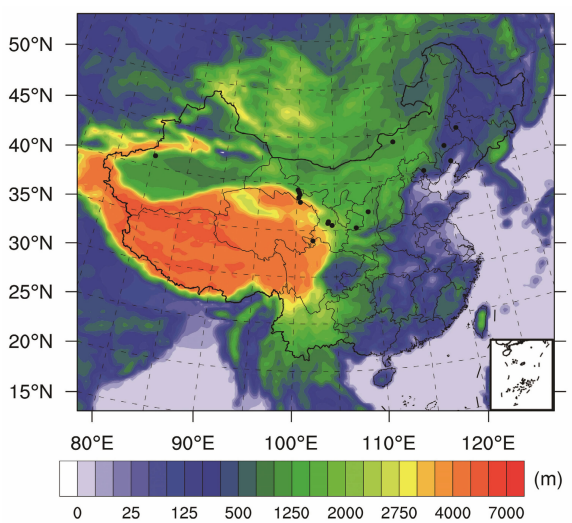

Figure 1. Model domain and topographic height (m). The dots represent the positions of the EC flux sites and the shading represents terrain height.

mean scale, the CAM and RRMTG schemes are close to the ERA-Interim circulation pattern, but without large differences in different radiation schemes.

4.2 *Validation using temperature and precipitation*

The WRF thermodynamic variables are not directly simulated at 2 m above ground, but instead are diagnosed from values at the land surface and the lowest model layers[4]. Fig. 2 shows the spatial distribution of annual mean 2-m air temperature difference between observation and simulation with different radiation schemes. Judging from the spatial distribution figure, the temperatures simulated using the three radiation schemes over eastern China underestimate, especially using the RRTM_DUDHIA scheme. The model runs that use the RRTM_GODDARD and RRTMG schemes simulate higher temperatures than the three other schemes, and thus show better agreement with observations. In addition, almost all of the schemes produce higher temperatures in Xinjiang Region and lower temperatures in some areas in northeastern China. For the seasonal change, the spring presents a similar pattern as the annual mean, while the difference spatial distribution of summer and winter demonstrate larger difference than that of autumn. The summer almost presents positive values over China, and the winter nearly has negative values in China. The different parameter setting may contribute a large portion to radiation simulation result.

The regional average temperature biases at different times (annual, summer and winter duration) are calculated between the different radiation schemes and the observed data over China (not shown). Our focus here is not to diagnose mean model biases, but rather to determine the differences in the biases among the different schemes relative to the observed temperature. As seen from the figure, the summer temperature bias changes are unlike those seen in the annual mean and winter mean. Almost all of the five sets of runs underestimate the annual mean and winter mean 2-m temperature, except for the RRTMG scheme; the New Goddard and RRTM_DUDHIA schemes underestimate the summer mean temperatures, whereas the other schemes overestimate those values. The above analysis indicates that RRTM_DUDHIA produces the largest biases, except in terms of summer temperature. More specifically, the annual mean results that best reproduce the observations are simulated by the RRTM_Goddard and RRTMG schemes, whereas the best summer mean temperatures are obtained using the RRTM and New Goddard schemes, and the RRTMG and New Goddard schemes are the best suited for simulating winter mean temperature. According to the results, one possible cause of the lower temperatures produced by RRTM would be the difference in the heat fluxes delivered by the surface layer scheme.

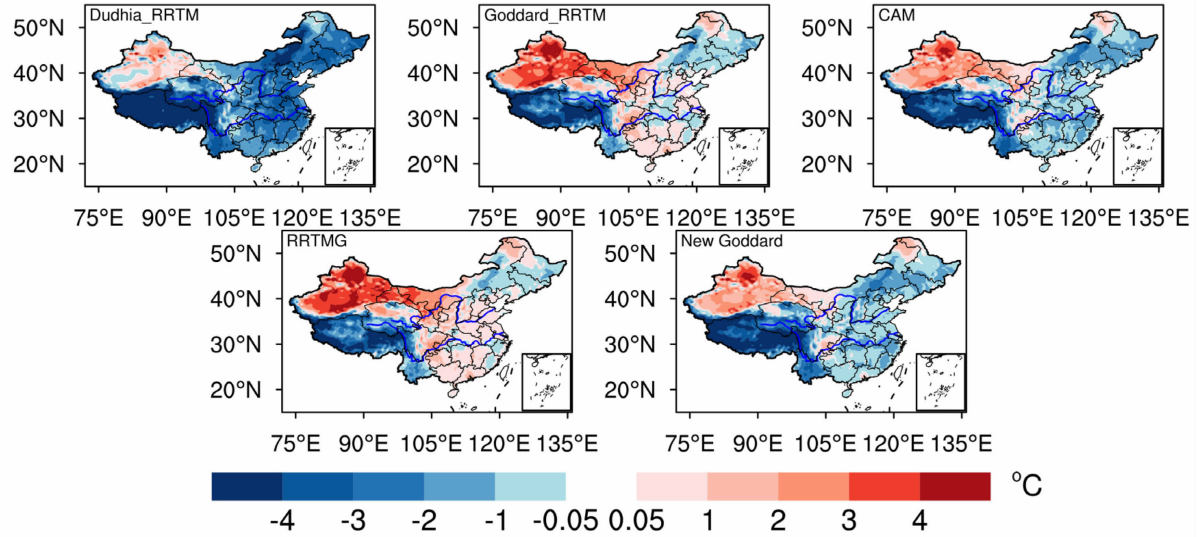

Figure 2. Spatial distribution of the annual mean temperatures difference (℃) during 2008, both from observations and as simulated using the five radiation schemes

The various radiation options in WRF show that the temperature differences can be significant. One of the reasons involves discrepancies among the radiation options in the preset concentrations of some trace gases, such as carbon dioxide. Hence the annual mean temperature differences simulated for three concentrations of carbon dioxide using the RRTMG radiation scheme show that the area of notable temperature changes caused by the carbon dioxide concentration is located in northern China (not shown).

The spatial distributions of annual mean precipitation difference between observation and simulation reproduced by the different radiation schemes are shown in Fig. 3. Based on the observed data, the amount of rainfall is less in the northwest and more in the southeast. Overall, the simulated rainfall amounts over China have overestimates, and the distribution contains a fictional center in the eastern part of the Tibet Plateau. The CAM scheme simulated the spatial distribution of precipitation better than the rest of the radiation schemes. The New Goddard scheme also simulated the precipitation distribution reasonably well, except for an underestimation over the middle reaches of the Yangtze River. Both the RRTMG and RRTM_GODDARD schemes overestimate precipitation over the south of China and northeastern China, while the RRTM_DUDHIA scheme underestimates precipitation in southern China. With regard to the seasonal pattern, except for the spring time, the left seasonal time have positive values over almost all of the China. The summer and winter time take the opposite pattern (winter: negative values; summer: positive values) in the south of China. For precipitation simulation, the high resolution is necessary for the good performance, in addition to the sophisticated data assimilation techniques.

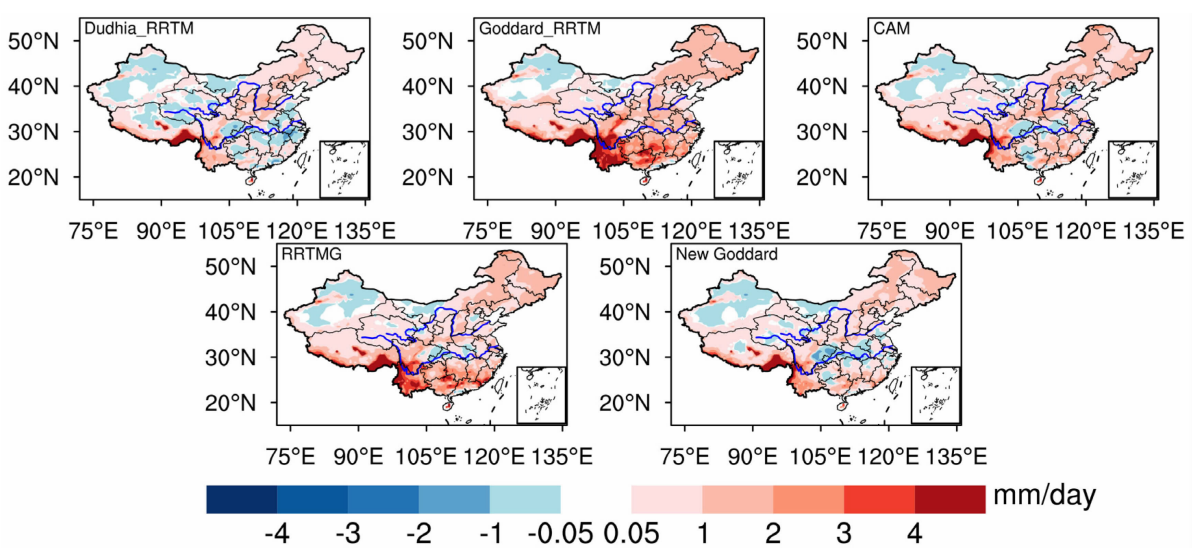

Figure 3. Spatial distribution of the simulated annual mean precipitation difference (mm/day) during 2008, both from observations and as simulated using the five radiation schemes.

Taylor diagrams are an excellent tool for displaying simulated fields together to effectively demonstrate how well they compare to observations and to track changes through the consideration of correlations, spatial standard deviations (normalized by the observed value), and root-mean-square errors(RMSEs)(Taylor[38]). Additionally, Taylor diagrams can summarize changes in the performance of individual models. The temperature and precipitation changes in different radiation schemes are displayed in Fig. 4. All the schemes present high temperature correlations, with values above 0.99. In contrast, the precipitation simulations are associated with somewhat larger differences in the standard deviations. The New Goddard scheme yields the best simulation; the worst reproduction is produced by the RRTM_Goddard scheme.

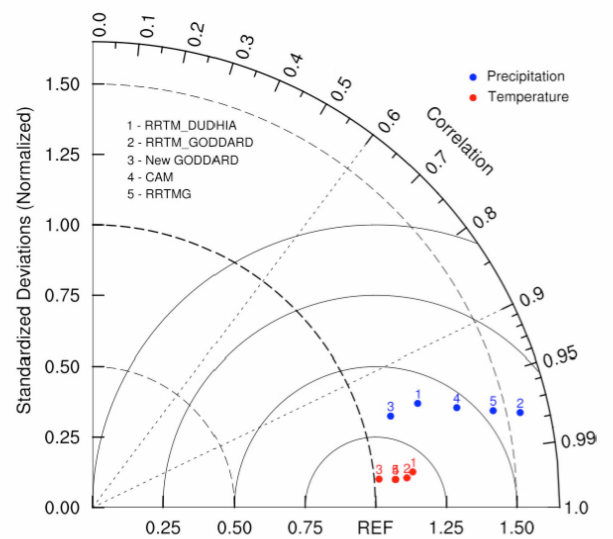

Figure 4. The Taylor diagram of annual mean temperature and precipitation simulated by different radiation schemes.

4.3 *Surface energy*

Turbulent heat fluxes include the sensible and latent heat fluxes, which can be directly calculated from eddy correlation, which is measured using appropriate equipment (Roberts[39]). As we know, the surface heat fluxes are largely sensitive to the height of the first model level. The first model level height is set at around 15 m above the ground in the experiments, and this design would result in reasonable simulation result. Based on the spatial distribution of annual mean sensible and latent heat flux between GLDAS data and the simulation results (Figure not shown), all of the schemes underestimate the sensible heat flux and overestimate the latent heat flux. Among the results, the CAM and New Goddard schemes are closest to the spatial distribution of the GLDAS data.

Another aspect of the performance of the surface layer schemes is the Bowen ratio, which is the ratio of surface sensible heat flux to the latent heat flux. Thus, in addition to the spatial distribution, the mean variations in the sensible and latent heat fluxes at EC flux sites (Yuzhong: one of the flux stations) are shown in Fig. 5. During the time period covered by the observations, the model runs with the different radiation schemes display a slightly higher sensible heat flux than the EC flux site value, and notable differences are observed around mid-summer. The latent heat flux demonstrates a similar change but with slightly higher difference in the summer.

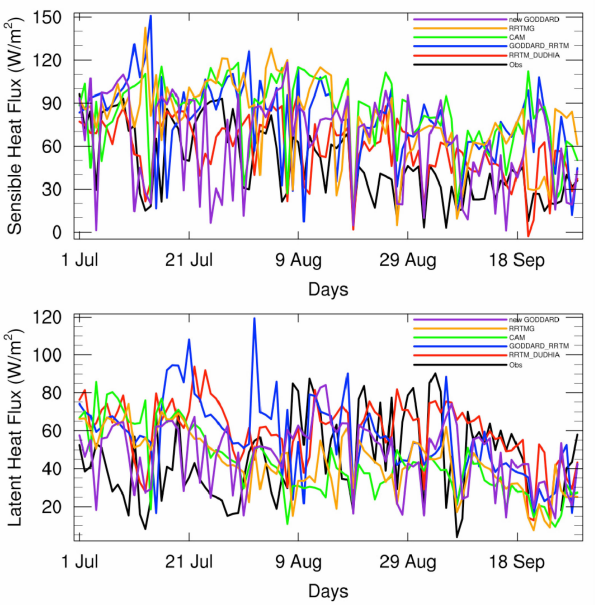

Figure 5. Comparison of mean time series of sensible flux and latent flux at Yuzhong EC flux site and simulation results for 1 July-30 September (top: sensible heat flux; bottom: latent heat flux).

The balance of energy and radiation is vital in the climate system. Net radiation is a critical variable for estimation of the surface energy budget(Bisht and Bras[40]). Therefore, net radiation from the different schemes is also compared to the GLDAS observations. It can be seen that the simulations with all sets of runs produced net radiation estimates that are slightly higher than the observed value, especially using the RRTM_Goddard and RRTMG schemes (Fig. 6). There are no obvious differences among the four seasons. After comparing the difference results on the annual mean or seasonal scale, the CAM and New Goddard schemes are found to give the best results. Collectively, the comparison of HFX, LH, and net solar radiation suggest that the differences in simulation performance between the different schemes is likely caused by cloud cover, the calculation of which is tied to a radiation option (since WRFv3.6, the calculation of cloud fraction has been independent of the radiation options).

4.4 *The PBL and low cloud cover*

Differences in vertical surface flux would result in differences in the distribution of the annual mean Planetary Boundary Layer (PBL) (Seidel et al.[41]). The annual mean variations in PBL heights (Fig. 7) are shown to indicate the dependence of the simulated boundary layer depth. The PBL heights reproduced by the CAM, New Goddard and RRTM_DUDHIA schemes are lower

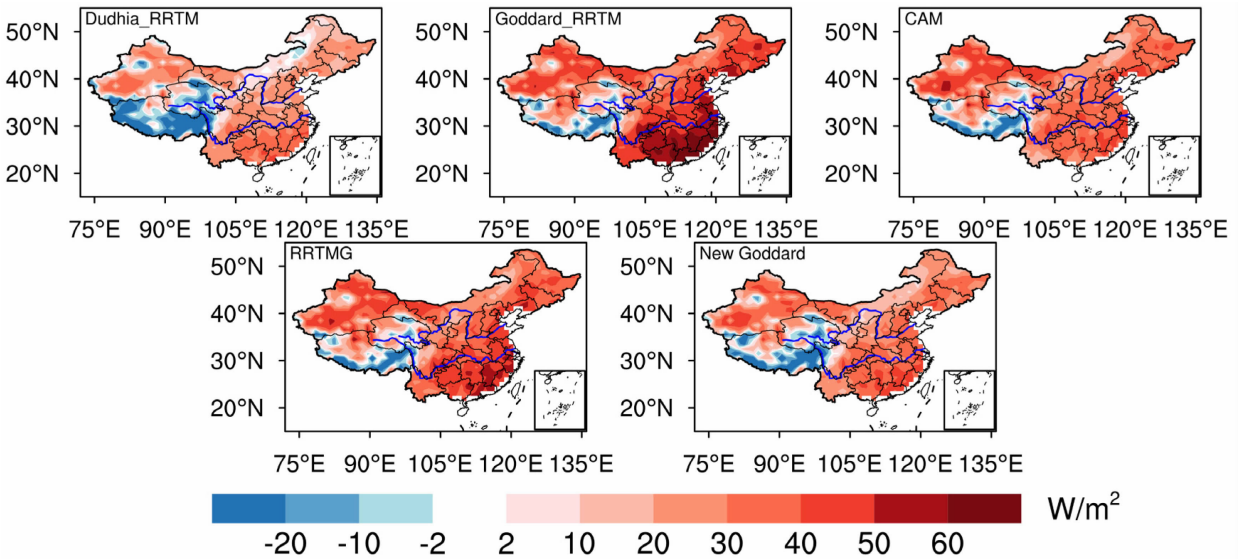

Figure 6. The simulated and observed annual mean net radiation difference spatial distribution (W/m^2).

than 500 m over most of eastern China. The PBL heights, as predicted with the RRTMG and RRTM_Goddard schemes, are higher than those predicted using the other schemes, which is consistent with the observation that the RRTMG and RRTM_Goddard simulate high annual mean temperatures. For the seasonal pattern in PBL, the winter has the lowest values with most areas less than 400 m and the PBL height in spring and autumn time almost all less than 600 m, among them, the summer address the most height values with more than 500 m.

Clouds reflect solar radiation and cool the surface of the Earth, and they also transmit incoming solar radiation; at the same time, they trap some of the outgoing infrared radiation emitted by the Earth and radiate it back downward, thereby warming the surface of the Earth. Clouds are considered as one of the largest uncertainties in models, both spatially and temporally (Rastogi et al.[42]). Thus, the accurate simulation of clouds is fundamental for determining radiative fluxes and many other meteorological variables. The impact of the interaction between clouds and radiation on transport is substantial, as the presence of clouds is the single biggest factor determining temperatures and the likelihood of ice/frost during winter nights. Besides, accurate radiation forecasts are of great importance for greenhouse effects. The output from WRF includes a 3-dimensional cloud cover in every sigma layer, and the low clouds are analyzed; these clouds are important in determining the surface energy balance. Referring to the definition of low cloud cover in ERA Interim, the fractions of cloud cover in the layers with sigma >0.8 are used to calculate the low cloud cover. The maximum fractional cloud cover in these layers is defined as the low cloud cover. These low cloud cover values are compared with those from ECWMF Interim (ERA-Interim) data[34]. From the spatial distribution of low cloud cover difference in the ERA-Interim data, low cloud cover is slight in northwest China, but substantial in the south, and high values occur in southwest China. The low cloud difference spatial distributions in northwestern China simulated by all the radiation schemes are fairly consistent with the observed one, and the minimum discrepancy is located in eastern China(Fig. 8). There is a little difference in the seasonal pattern, the summer and winter has the opposite value in the south of the Yangtze River. The autumn and spring show a similar pattern as that of the annual mean.

In the seasonal scale, the simulated temperature spatial distribution is well consistent with the low cloud cover, and the precipitation is also impacted by the low cloud cover.

5 CONCLUSIONS AND DISCUSSION

A series of simulations spanning one year has been conducted with WRF using different radiation schemes (RRTM_DUDHIA, RRTM_Goddard, New Goddard, CAM and RRTMG) in China during 2008 are evaluated. The temperature differences between the radiation schemes are small, based on the annual spatial distribution and Taylor diagram. Notably, use of the RRTM_DUDHIA scheme produces the largest bias, and the RRTMG scheme is the best one in terms of simulated temperature. As for the annual mean rainfall distribution, the New Goddard and CAM scheme are the excellent ones.

For the turbulent flux, all of the schemes overestimate the sensible heat flux and the latent heat flux. Among the schemes, the CAM scheme produces results that are closest to the GLDAS spatial distribution. The PBL heights predicted with the RRTMG and RRTM_Goddard scheme are higher than those predicted by the other schemes, which corresponds to the simulated temperature distribution. The calculation of annual mean low cloud cover is tied to a radiation option. The spatial distribution in the northwest is reproduced by all the

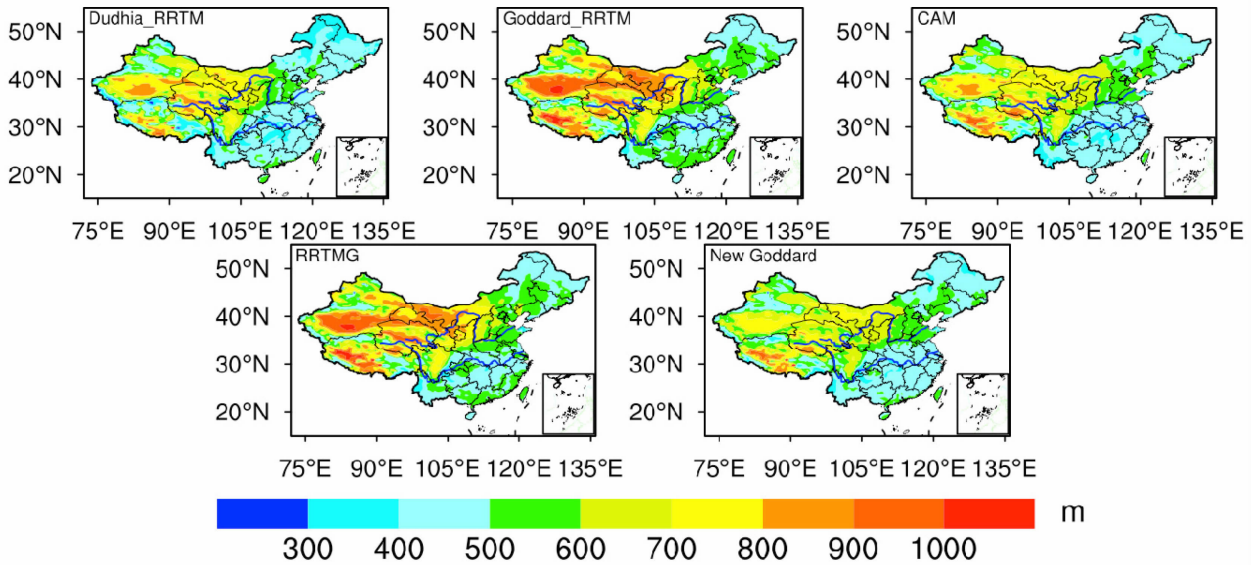

Figure 7. The annual mean PBL height simulated by different radiation schemes (m).

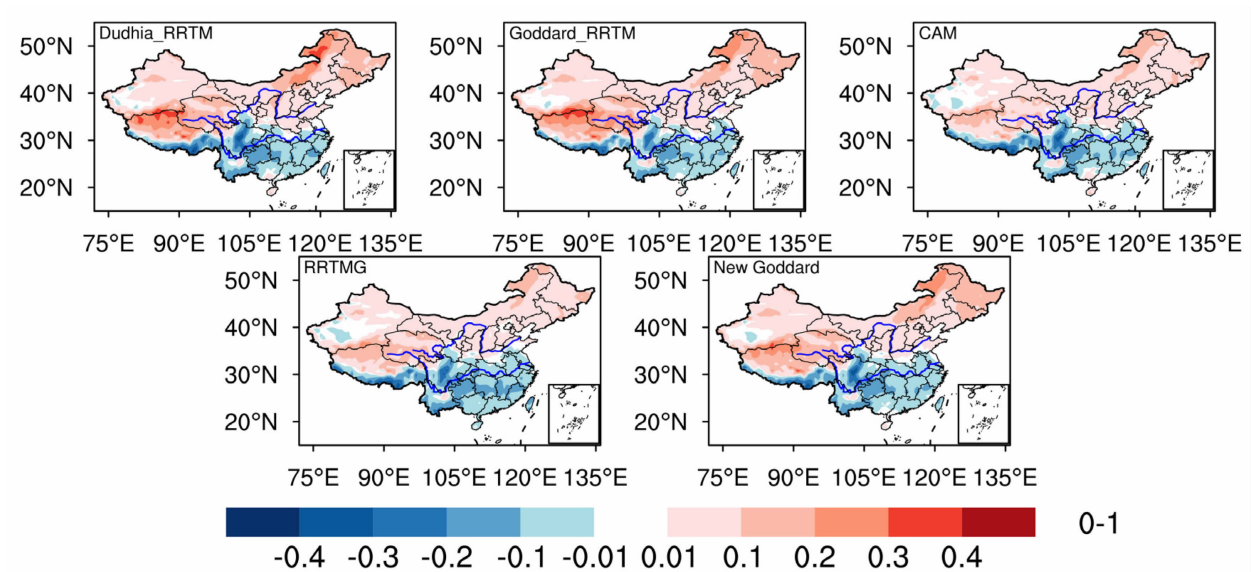

Figure 8. The spatial distribution of annual mean low cloud cover difference (fraction).

radiation schemes and is almost consistent with that of ERA-Interim, and the minimum differences are located in eastern China.

The simulated temperature spatial distribution shows better consistency with the low cloud cover, either on the annual or seasonal scale. The precipitation also presents good relationship with low cloud cover.

The accuracy of the radiative transfer is also sensitive to the accuracy of the atmospheric state input to the radiation calculation. It is particularly sensitive to the specification of cloud properties and cloud amount, which requires further evaluation in the WRF model. Significant differences in surface fluxes and radiation relative to observations may be due either to differences in the algorithmic accuracy of each radiation code or the treatment or concentrations of trace gases, which vary among the radiation options.

Except the different radiations, the resolution, nesting and nudging options also largely impact the simulation results. As for our daily temperature simulation compared with the Beijing station data, the temperature differences could reach 2 degrees. Combining all the factors results, the New Goddard and CAM radiation schemes are the best simulation ones, but for high resolution and nesting results, there may be different results. More detailed comparisons are needed.

REFERENCES:

[1] GIORGI F, MEARNS LO. Introduction to special section: Regional climate modeling revisited [J]. J Geophys Res: Atmos, 1999, 104(D6): 6335-6352.

[2] KIM H J, CHUNG I U, LEE K T. Effects of an advanced radiation parameterization on a troposphere-stratosphere AGCM simulation [J]. Asia-Pacific J Atmos Sci, 2009, 45

(4): 439-462.
[3] FENG J, WANG Y, MA Z. Long-term simulation of large-scale urbanization effect on the East Asian monsoon [J]. Clim Change, 2015, 129(3-4): 511-523.
[4] FENG J, WANG Y, MA Z, et al. Simulating the regional impacts of urbanization and anthropogenic heat release on climate across China [J]. J Climate, 2012, 25 (20): 7187-7203.
[5] HEATH N K, FUELBERG H E. Using a WRF simulation to examine regions where convection impacts the Asian summer monsoon anticyclone [J]. Atmos Chem Phys, 2014, 14(4): 2055-2070.
[6] HU X, NIELSEN-GAMMON J W, ZHANG F. Evaluation of three planetary boundary layer schemes in the WRF model [J]. J Appl Meteor Climatol, 2010, 49 (9): 1831-1844.
[7] BANKS R F, JORDI T A, JOSE M B, et al. Sensitivity of boundary-layer variables to PBL schemes in the WRF model based on surface meteorological observations, lidar, and radiosondes during the HygrA-CD campaign [J]. Atmos Res, 2016, 176-177: 185-201.
[8] COHEN A E, CAVALLO S M, CONIGLIO M C, et al. A Review of planetary boundary layer parameterization schemes and their sensitivity in simulating southeastern U. S. cold season severe weather environments [J]. Wea Forecasting, 2015, 30(3): 591-612.
[9] HUANG H, HALL A, TEIXEIRA J. Evaluation of the WRF PBL parameterizations for marine boundary layer clouds: Cumulus and stratocumulus [J]. Mon Wea Rev, 2013, 141(7): 2265-2271.
[10] WANG Zi-qian, DUAN An-min, WU Guo-xiong. Impacts of boundary layer parameterization schemes and air-sea coupling on WRF simulation of the East Asian summer monsoon [J]. Sci China Earth Sci, 2014, 57 (7): 1480-1493.
[11] ZHANG C, WANG Y, HAMILTON K. Improved representation of boundary layer clouds over the southeast Pacific in ARW-WRF using a modified Tiedtke cumulus parameterization scheme [J]. Mon Wea Rev, 2011, 139(11): 3489-3513.
[12] ARAKAWA A. The cumulus parameterization problem: Past, present, and future [J]. J Climate, 2004, 17 (13): 2493-2525.
[13] KAIN J S, FRITSCH J M. A one-dimensional entraining/detraining plume model and its application in convective parameterization [J]. J Atmos Sci, 1990, 47 (23): 2784-2802.
[14] ARAKAWA A, SCHUBERT W H. Interaction of a cumulus cloud ensemble with the large-scale environment, Part I [J]. 1974, 31(3): 674-701.
[15] ZHANG M, LIN W, KLEIN S, et al. Comparing clouds and their seasonal variations in 10 atmospheric general circulation models with satellite measurements [J]. J Geophys Res: Atmos, 2005, 110(15): 1-18.
[16] DUDHIA J. Numerical study of convection observed during the winter monsoon experiment using a mesoscale two-dimensional model [J]. J Atmos Sci, 1989, 46(20): 3077-3107.
[17] STEPHENS G L. Radiation profile in extended water clouds II: Parameterization schemes [J]. J Atmos Sci, 1978, 35(11): 2123-2132.
[18] CHOU M D, LEE K T, TSAY S C, et al. Parameterization for cloud longwave scattering for use in atmospheric models [J]. J Climate, 1999, 12(1): 159-169.
[19] IACONO M J, MLAWER E J, CLOUGH S A, et al. Impact of an improved longwave radiation model, RRTM, on the energy budget and thermodynamic properties of the NCAR community climate model, CCM3 [J]. J Geophys Res: Atmos, 2000, 105 (D11): 14873-14873.
[20] RAISANEN P, BARKER H W, COLE JNS. The Monte Carlo independent column approximation's conditional random noise: Impact on simulated climate [J]. J Climate, 2005, 18(22): 4715-4730.
[21] IACONO M J, DELAMERE J S, MLAWER E J, et al. Radiative forcing by long-lived greenhouse gases: Calculations with the AER radiative transfer models [J]. J Geophys Res Atmos, 2008, 113(13), doi: 10.1029/2008JD 009944.
[22] NEALE R B, CHEN C C, GETTELMAN A, et al. Description of the NCAR community atmosphere model (CAM5.0) [R]. Note NCAR/Tn-486+STR, 2010, 1 (1): 1-12.
[23] GU Y, LIOU KN, OU S C, et al. Cirrus cloud simulations using WRF with improved radiation parameterization and increased vertical resolution [J]. J Geophys Res: Atmos, 2011, 116(6), doi: 10.1029/2010JD 014574.
[24] HONG S Y, DUDHIA J, CHEN S H. A revised approach to ice microphysical processes for the bulk parameterization of clouds and precipitation [J]. Mon Wea Rev, 2004, 132(1): 103-120.
[25] KAIN J S. The Kain-Fritsch convective parameterization: An update [J]. J Appl Meteor, 2004, 43(1): 170-181.
[26] HONG S, NOH Y, DUDHIA J. A new vertical diffusion package with an explicit treatment of entrainment processes [J]. Mon Wea Rev, 2006, 134(9): 2318-2341.
[27] CHEN F, DUDHIA J. Coupling an advanced land surface–hydrology model with the Penn State–NCAR MM5 modeling system, Part I: Model implementation and sensitivity [J]. Mon Wea Rev, 2001, 129 (4): 569-585.
[28] SAIDE P E, SPAK S N, CARMICHAEL G R, et al. Evaluating WRF-Chem aerosol indirect effects in Southeast Pacific marine stratocumulus during VOCALS-Rex [J]. Atmos Chem Phys, 2012, 12 (6): 3045-3064.
[29] YANG Q, WI GUSTAFSON J R, FAST J D, et al. Assessing regional scale predictions of aerosols, marine stratocumulus, and their interactions during VOCALS-REx using WRF-Chem [J]. Atmos Chem Phys, 2011, 11(23): 11951-11975.
[30] YU S, MATHUR R, PLEIM J, et al. Aerosol indirect effect on the grid-scale clouds in the two-way coupled WRF-CMAQ: Model description, development, evaluation and regional analysis [J]. Atmos Chem Phys, 2014, 14(20): 11247-11285.
[31] MONTORNES A, CODINA B, ZACK J W. Analysis of the ozone profile specifications in the WRF-ARW model and their impact on the simulation of direct solar radiation [J]. Atmos Chem Phys, 2015, 15(5): 2693-2707.
[32] XIE P, CHEN M, YANG S, et al. A Gauge-based analysis of daily precipitation over East Asia [J]. J Hydrometeor, 2007, 8(3): 607-626.

[33] XU Y, GAO X, SHEN Y, et al. A daily temperature dataset over China and its application in validating a RCM simulation [J]. Adv Atmos Sci, 2009, 26 (4): 763-772.

[34] DEE D P, UPPALA S M, SIMMONS A J, et al. The ERA-Interim reanalysis: Configuration and performance of the data assimilation system [J]. Quart J Roy Meteor Soc, 2011, 137(656): 553-597.

[35] WANG H, JIA G, FU C, et al. Deriving maximal light use efficiency from coordinated flux measurements and satellite data for regional gross primary production modeling [J]. Remote Sensing Environ, 2010, 114(10): 2248-2258.

[36] HOU Jiang-tao, JIA Gen-suo, ZHAO Tian-bao, et al. Satellite-based estimation of daily average net radiation under clear-sky conditions [J]. Adv Atmos Sci, 2014, 31 (3): 705-720.

[37] ZENG X, SHAIKH M, DAI Y, et al. Coupling of the common land model to the NCAR community climate model [J]. J Climate, 2002, 15(14): 1832-1854.

[38] TAYLOR KE. Summarizing multiple aspects of model performance in a single diagram [J]. J Geophys Res: Atmos, 2001, 106(D7): 7183-7192.

[39] ROBERTS JB, ROBERTSON FR, CLAYSON CA, et al. Characterization of turbulent latent and sensible heat flux exchange between the atmosphere and ocean in MERRA [J]. J Climate, 2012, 25(3): 821-838.

[40] BISHT G, BRAS RL. Estimation of net radiation from the MODIS data under all sky conditions: Southern Great Plains case study [J]. Remote Sensing Environ, 2010, 114 (7): 1522-1534.

[41] SEIDEL DJ, AO CO, LI K. Estimating climatological planetary boundary layer heights from radiosonde observations: Comparison of methods and uncertainty analysis [J]. J Geophys Res: Atmos, 2010, 115(D16), doi: 10.1029/2009JD013680.

[42] RASTOGI B, WILLIAMS A P, FISCHER D T, et al. Spatial and temporal patterns of cloud cover and fog inundation in coastal California: Ecological implications [J]. Earth Interact, 2016, 20(15): 1-19.

Citation: WANG Yong-li, FENG Jin-ming, ZHENG Zi-yan, et al. Sensitivity of the weather research and forecasting model to radiation schemes in China [J]. J Trop Meteor, 2019, 25(2): 201-210.